Concurrent removal of hardness and fluoride in water by monopolar electrocoagulation

J.U. Halpegama [a,b,e], K.Y. Heenkenda [a], Zhiguo Wu [a,b], K.G.N. Nanayakkara [c], R.M. G. Rajapakse [d], A. Bandara [d], Ajith C. Herath [e], Xing Chen [f], Rohan Weerasooriya [a,f,*]

[a] National Centre for Water Quality Research, National Institute of Fundamental Studies, Hanthana, Kandy 20000, Sri Lanka
[b] Postgraduate Institute of Science, University of Peradeniya 20400, Sri Lanka
[c] Department of Civil Engineering, Faculty of Engineering, University of Peradeniya 20400, Sri Lanka
[d] Department of Chemistry, Faculty of Science, University of Peradeniya 20400, Sri Lanka
[e] Department of Chemical Sciences, Faculty of Applied Sciences, Rajarata University of Sri Lanka, Mihintale 50300 Sri Lanka
[f] Industry and Equipment Technology Institute, Hefei University of Technology, Hefei 230009, PR China

ARTICLE INFO

ABSTRACT

Water treatment based on electrocoagulation (EC) is attractive since required chemicals and colloids are produced in-situ. However, optimisation of EC operation parameters is necessary to enhance its efficiency. We optimised EC cell parameters by the response surface method (RSM). The optimal removal efficiencies of hardness (63%) and fluoride (97%) were achieved at 1.98 kW h/m^3. With the removal of divalent cations, some anionic species concurrently remove via an energetically feasible route to adjust the charge balance. When simulated water is used (450 mg/L TDS, 580 mg/L CaCO$_3$, 10 mg/L fluorides and pH 6.50), 83% hardness and 99% fluoride are removed with 0.69 kW h/m^2 energy consumption. The chemical species in the solution matrix, particularly SO$_4^{2-}$, significantly affect the hardness and fluoride removal efficiencies. The contaminated EC sludge resulted from feed water is characterised by spectroscopic methods to probe hardness and fluoride removal mechanisms. In the presence of Mg^{2+}, F$^-$ interacts with Al-sludge sites forming $\equiv$MgF$-$OH. When Ca^{2+} and F$^-$ are present, both $\equiv$CaF$-$OH and $\equiv$CaF are formed. In Ca^{2+}, Mg^{2+} and F$^-$ treated Al-sludge dominates $\equiv$CaF$-$OH and $\equiv$CaF over $\equiv$MgF$-$OH.

1. Introduction

Due to intense rock weathering in the tropics, the natural groundwater enriches lithogenic solutes as fluoride and hardness (viz., divalent cations). The adverse climatic conditions prevailing in these regions force people to consume large quantities of solutes-enriched water, often implicating severe health problems [1–3]. Fluoride is an enforceable primary water quality standard [4] (maximum contaminants limit, MCL 1.5 mg/L). Hardness is a non-enforceable secondary water quality standard where no MCL is defined. However, hardness (and TDS) renders water unpalatable, restricting its human consumption [2]. Therefore, improvement of palatability of the drinking water is essential before treating excess trace solutes as fluoride. When water hardness (Ca^{2+} and Mg^{2+}) is removed, anions in solution may adjust their

activities to restore charge balance via energetically feasible pathways. Therefore, eliminating major cations in water is required first, and then assess other contaminants in the treated water to determine additional treatment, if needed.

Hardness can be removed by reverse osmosis (RO) or nano-membranes (NM), ion exchange resins, lime softening, and electrochemical methods [5,6]. In RO technology, almost all solutes in water are removed; hence, the treated water becomes unpalatable due to a lack of solutes. Long-term consumption of solutes-deficient water may also lead to nutritional disorders [7,8]. In lime softening, excess sludge is generated, and the treated water also requires additional treatment. The ion exchange plants generate high TDS water enriched with Na$^+$ that need different treatment [9,10]. In contrast, the electrochemical methods can provide a solution for concurrent removal of fluoride and

hardness. Two types of electrochemical methods, i.e., electrodialysis self-reversal (EDR) and electrocoagulation (EC), are used to remove hardness, fluoride or other solutes in water [11,12]. By EDR technology, the hardness in water removes efficiently; however, they show limited success in removing fluoride. The fluoride in water replaces OH⁻ on the membrane, forming specific bonds with the membrane sites, which the EDR self-reversal process cannot regenerate. The disposal of liquid EDR concentrates poses an additional issue [13–16]. The electrocoagulation method can be treated as a unification of several water treatment processes, e.g., coagulation, sedimentation, flotation, and oxidation [17]. Unlike membrane technology, in EC, the composition of the inlet water does not require rigorous pretreatment to remove particulates, natural organic matter, etc. [18,19]. The EC technology can remove inorganic ions, organic compounds, colour, oil, grease, and turbidity in water [20]. Further, the EC can destruct microbes via cell rupturing under an electric flux [21]. The sludge generated in EC is compact due to minimal enrichment of ions in solution and floats by gas bubbles generated at the cathode [22]. Electrocoagulation technology is not complex compared to membrane or EDR methods, and the routine operation is straightforward. Hence, compared to membrane technology or EDR, EC methods are simple, robust, chemical-free, and cost-effective [19, 23–25].

Electrocoagulation does not require external coagulants since they generate in situ by dissolving metal anodes. Compared to Fe, the Al electrodes used in EC cells is profitable for the following reasons: irrespective of the current flux, Fe corrodes spontaneously in water; hence the generation of Fe derived coagulants is uncontrolled. However, the Al electrodes undergo surface passivation by forming an Al_2O_3 layer, and under controlled current flux water $[Al^{3+}]$ can regulate; unlike Fe^{3+}, the Al^{3+} undergoes polymerisation forming $Al(OH)_{15}^{3+}$, $Al_7(OH)_{17}^{4+}$, $Al_8(OH)_{20}^{4+}$ and, $Al_{13}O_4(OH)_{24}^{7+}$ therefore, the presence of free Al^{3+} is limited [19,26]. The required Al derived coagulants can control the demand; hence the sludge production and alum addition can cut off substantially. Therefore, we used Al sacrificing anode in EC to examine concurrent hardness and fluoride removal in water. The water hardness is removed by precipitating divalent ions on the cathode and adsorption onto $Al(OH)_{3n}$ flocs produced by the EC cell in near-neutral pH [5,19,27] (e.g. pH 6–8). In determining the effect of Ca^{2+} or Mg^{2+} on defluoridation an optimal value is observed in the presence of Mg^{2+} by forming an $Mg(OH)_2$ coating on Al-derived colloids that results in low F⁻ retention affinity. The difference in EC defluoridation between Ca^{2+} and Mg^{2+} is known to depend on flocs composition. However, the synergy between Ca^{2+} and Mg^{2+} on defluoridation requires a detailed study. Mostly the EC methods are used to remediate a single contaminant as fluoride in water. Its versatility in removing multiple pollutants in drinking water is also demonstrated. The EC cells with Fe-Al anode are used to remove Sb and As [28] or As and F [29]. The substitution of Fe^{3+} ions by Al^{3+} ions in the solid surface resulted in increased surface sites for the adsorption of pollutants. However, the concurrent production of aluminium and iron derived colloids may result in excess wastes that require additional treatment [28]. Guzman et al. report the efficient removal of fluoride and arsenate in natural water using EC with Al anodes where ion exchange and adsorption co-occur for fluoride and arsenic removal, respectively [30]. In this case, however, the water hardness is low (9.8 mg/L).

We optimised EC cell parameters for concurrent removal of hardness (e.g., Ca^{2+} Mg^{2+}) and fluoride in groundwater. We first optimised the EC cell for hardness removal efficiency in the presence of fluoride in water. The ions removal efficiency depends on water quality (pH, ionic strength, temperature, TDS) and EC cell (electrode dimension, applied current and voltage, processing time) parameters. The performance of EC cell depends markedly on the cell parameters compare to water quality. The optimisation of EC cell parameters first requires a systematic approach for major solutes (in this case, hardness) in water. Once the optimisation is achieved, the composition of the treated water

Table 1
Chemical composition of simulated and groundwater samples.

Sample type and location	pH	EC µS/cm	TDS mg/L	Total hardness mg/L CaCO₃	Fluoride mg/L
Simulated water ($Ca^{2+}_{(aq)}$, $Mg^{2+}_{(aq)}$ and $F^-_{(aq)}$)	6.5	970	450	580	10
L-1 (8°21′11.3″ N, 80°30′07.9″ E)	6.6	970	470	183	0.45
L-2 (8°19′53.9″ N, 80°36′04.1″ E)	7.1	750	380	291	0.48

requires assessment for trace constituents (in this case, fluoride). We used a multi-factorial method based on response surface method (RSM) to optimise the current flux and reaction time for optimal hardness removal in water [31]. The response variable is only a function of a singly varied parameter. Therefore, the desired independent variables can be combined, and their mutual interactions can also evaluate for optimisation [32]. Besides, the RSM method decreases the total number of experiments required to optimise by saving time and experimental costs, providing an additional advantage. However, the optimisation process optimises operational conditions without shedding light on hardness or fluoride mechanisms [33]. At optimal conditions, the Al-derived sludge generated by the EC was analysed by spectroscopic methods to elucidate fluoride and hardness removal mechanism.

2. Materials and methods

2.1. Materials

The aluminium plates (98% purity) required for EC cell design were obtained from Spectra Industries Lanka (Pvt) Ltd. Analytical grade, A.R., NaF, $MgCl_2$, $CaCl_2$. $2H_2O$, HNO_3 and $NaClO_4$ were obtained from Sigma Aldrich (USA). Milli Q water (Thermo ultra-pure system, Hungary 0.055 µS/cm) was used in sample preparation. The required groundwater samples for experiments were collected from two villages within the same climatic zone in Sri Lanka. (The detailed chemical composition of the water samples is shown in Table 1-S; support documentation). For optimisation experiments, a simulated water sample was prepared to match the hardness and fluoride of the natural water using NaF, $MgCl_2$, $CaCl_2$. $2H_2O$ and $NaClO_4$ with a controlled matrix. Table 1 shows the chemical composition of the water samples used.

2.2. Methods

2.2.1. Lab-scale batch electrocoagulation reactor

A laboratory-scale cylindrical batch reactor (Pyrex cell: diameter 6.4 cm and height 8.00 cm) was used in the experiments. Two plates of aluminium (dimensions 6.00 cm × 1.60 cm × 0.44 cm; immersion depth 5.30 cm) were used as electrodes. The net capacity of the EC reactor was 175 mL. The two electrodes were connected in a monopolar configuration. The gap between the electrodes was maintained at 1.00 ± 0.01 cm. Regulated current supply was given with high precision DC power supply (ZHAOXIN PS 305D; resolution voltage-0.1 V [stability $\leq 0.01\% + 2$ mV], current-0.01 A [stability $\leq 0.1\% + 3$ mA]. Before each experiment, electrodes were rubbed with sandpaper to remove scale and soaked in 1 M HNO_3 and Mill Q water for surface cleaning. The EC cell with monopolar electrode configuration, thus designed was used to optimise process time and current density for water hardness removal according to the method discussed in Section 2.2.2.

2.2.2. Electrochemical cell parameters optimisation

Response surface method was used for the statistical design of the experiments to evaluate the optimum EC cell operational parameters (process time: X_1 and current density: X_2) to maximise water hardness

Table 2
Central composite design observations of independent variables and predicted and experimentally achieved hardness removal efficiency used for the optimisation.

Independent factors	Factor		Range and level	
	X		Low (−1)	High (+1)
Time (min)	X_1		10	45
Current density (A/cm^2)	X_2		0.117	0.353

Design variables

Run order	Actual levels		Observations - hardness removal efficiency (%)	
	Time (min)	Current density (mA/cm^2)	L - 1	L - 2
1	52.2	3.53	63	64
2	45	2.35	57	59
3	27.5	4.71	48	52
4	27.5	4.71	48	52
5	10	5.89	35	41
6	27.5	4.71	42	51
7	2.7	4.71	38	31
8	10	2.35	38	37
9	27.5	4.71	51	53
10	27.5	4.71	54	54
11	45	5.89	62	59
12	27.5	7.07	48	53
13	27.5	1.17	48	54

removal efficiency, Y_1 according to the following model.

$$Y = \beta_0 + \sum_i \beta_i X_i + \sum_i \beta_{ij} X_i^2 + \sum_{i>j} \beta_{ij} X_i X_j$$

where Y response function (hardness removal efficiency), β_0 is intercept, β_i and β_{ij} are linear and quadratic coefficients, β_{ij} accounts for X_i and X_j, and X_i and X_j are independent factors, i.e., current density and process time. Based on initial experiments, the initial values of independent variables are shown in Table 2. According to the central composite design (CCD) developed by Minitab code, a possible combination of experimental protocols was obtained. Accordingly, thirteen experimental protocols were used to evaluate response function experimentally (Table 2). The model optimisation was carried out with the natural water collected from the L-1 (Table 1). Afterwards, the model validation was carried out with the natural water sample collected from L-2 from the same climatic zone. After that the validated model was used to simulate the chemical composition of the stimulated water.

2.2.3. Water quality assessments and sludge characterisation

The samples' pH and electrical conductivity (TDS calculated) were measured by a multi-parameters analyser (HANNA HI 9811-5, USA). Cations in solution were measured by inductively coupled plasma optical emission spectrometer (ICP-OES) (ICPA 7000, Thermo, USA) using certified standard solutions for calibration. Fluoride in solution was analysed using ion chromatography (Shimadzu, Japan) equipped with the conductivity detector (Shimadzu CDD 10A VP, Japan) and autosampler. Quality control data of the measurements made by IC and ICP-OES as described elsewhere [34–36]. The spike recoveries of fluoride hardness were measured using NIST CRN anion solution (ROTH multi-element IC CAS 2668). In water, 97.83 ± 0.06% recoveries were obtained for fluoride. For calcium and magnesium detection, ICP CRN was used (TRaceCERT 54704 Siga Aldrich, USA), and the spike recoveries are 100.3 ± 1.51% and 98 ± 1.76% for calcium and magnesium, respectively. The transmission FTIR method was used to characterise the Al sludge generated by EC experiments. KBr pellets were prepared at 1:10 sample: KBr ratio. Transmission FTIR spectra
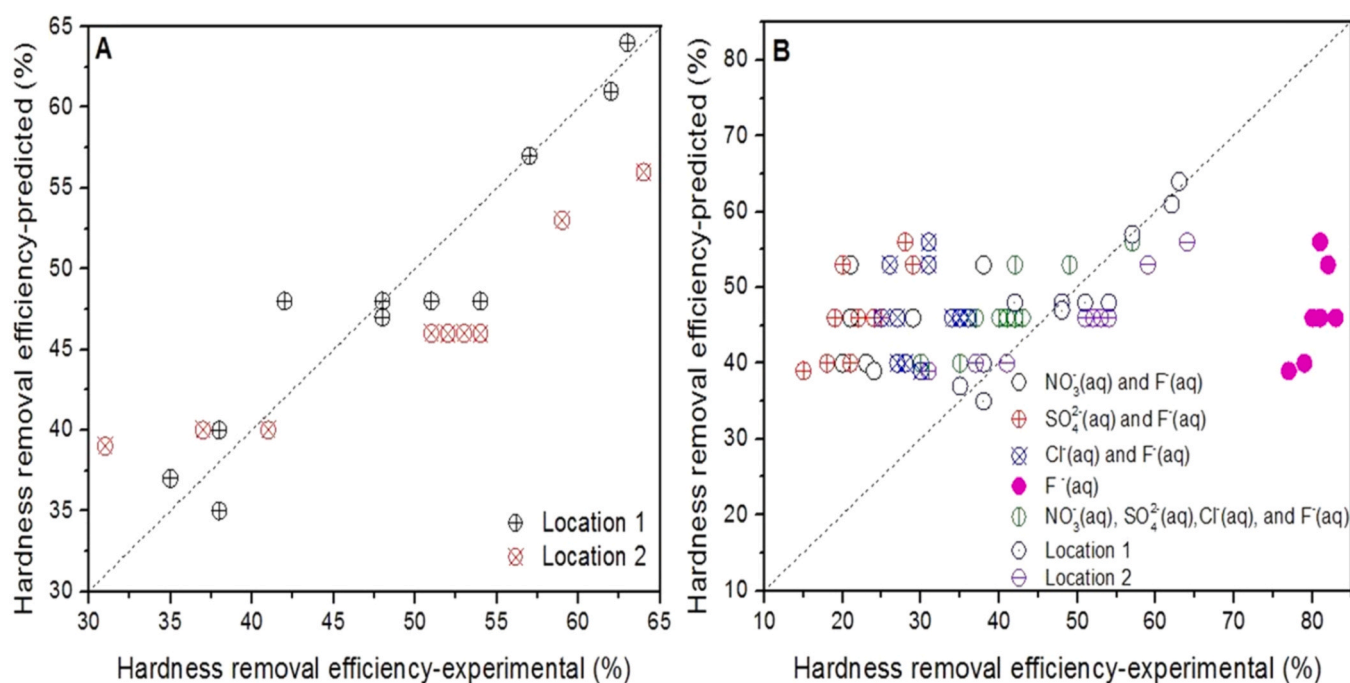

Fig. 1. Variations of hardness removal efficiency in A. groundwater of locations 1 and 2; symbols represent observations. Source water composition, current density and response time were related to Table 1 and 2. B. Simulated water by EC. Symbols represent various simulated water types. Model calculations were carried out with an RMS model developed for natural groundwater.
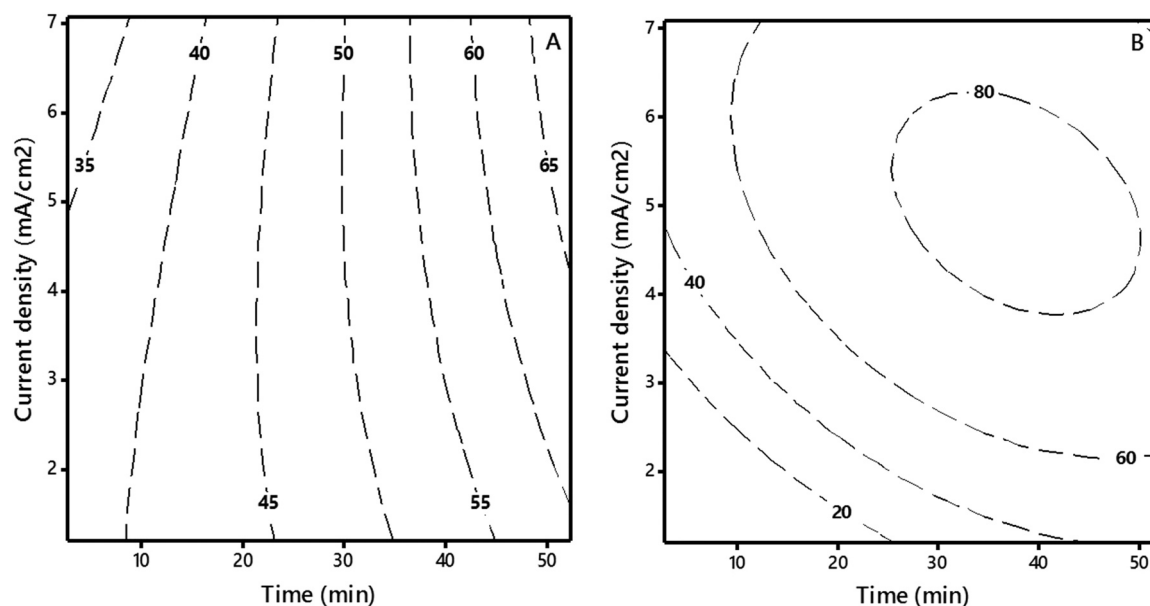
Fig. 2. Variation of hardness and fluoride removal efficiencies as a function of current density and process time. A. hardness B. fluoride as a function of time and current density for location 1. Source water composition: TDS 470 mg/L, hardness 183 mg/L $CaCO_3$, fluoride 0.45 mg/L and pH 6.60.

were recorded with an IR spectrometer with a DTGS detector (iS50 Thermo Scientific, USA). All spectra were obtained at 4 cm^{-1} resolutions in the 400 – 4000 cm^{-1} spectral range. X-ray diffractograms of aluminium sludge were obtained for phase identification. An X-ray diffractometer at 20 kV and 30 mA was operated using Cu-Kα radiation at $\lambda = 0.154$ nm (Bruker D8 Advance Eco). X-ray photoelectron spectroscopy (XPS) measurements were carried out using a Thermo Esca lab 250Xi (Thermo Fisher Scientific, Waltham, MA, USA) system using a monochromatic Al Kα source (1320 eV, 140 W). Peak fitting was performed according to Gaussian/Lorentzian functions using Origin Pro 9 software. The EC sludge morphology and surface structures were observed by cold field emission scanning electron microscope (Hitachi, Japan; SU8020).

3. Results and discussion

3.1. Central composite design model development for hardness removal

The efficiency of treating contaminants by EC depends on both feed water composition, viz., pH, ionic strength, contaminants load, and EC cell parameters, viz. current and process time. Hardness occurs mainly due to major divalent cations as Ca^{2+} and Mg^{2+} in water. To ensure drinking water palatability, the major species (presently Ca^{2+} and Mg^{2+}) require treating first; however, to ensure solution charge balance, anions' concentration automatically adjusts. We designed experiments to optimise EC cell parameters to maximise hardness removal in natural groundwater by RSM. The central composite design of independent design variables, viz. current density and time, are shown in Table 2. The coefficients of the response function for hardness removal efficiency is shown in Table 2-S. The ANOVA data of independent design factors indicate that the RSM regression model adequately interprets observations (F = 11.80 Table 3-S), and the hardness removal efficiency ranges between 35% and 63%. Statistical analysis showed the significance of the linear term (X_1, time) in the model with P_r (probability) < 0.05 (Table 3-S). However, the coefficients correspond to linear (X_1), square (X_1^2) and cross-term interactions (X_1X_2) are not significant (P(r)> 0.05). Accordingly, the optimised RSM model for hardness removal efficiency in water is shown below:

$$(Y_1) = 38.4 + 0.170X_1 - 0.36X_2 + 0.00324X_1^2 - 0.122X_2^2 + 0.0570(X_1X_2) \quad (1)$$

$$(S = 3.78, R^2 = 89.39\%, R_{adj}^2 = 81.81\%, \ R_{pre}^2 = 71.08\%)$$

The suitability of the RSM model in response function predictions is embedded in the response variable (S), regression coefficient (R^2), R^2 adjusted, and R^2_{pre} predicted values. The high regression coefficient (R^2 = 89.39%) and its agreement with adj. R^2 complies with a good data fit. The S value measures the agreement between data values and response surface. A minimal S value implies a good agreement between measurements and modelled data [32,37]. Experimental error of hardness removal efficiency as shown by lack of fits is statistically insignificant (Pr(probability > 0.05), and the model adequately predicts observations with 6% uncertainty [37] (Table 3-S). The optimised RSM model was then validated using an independent dataset from a different location in the same climatic zone (viz. L-2). Accordingly, the hardness removal efficiency values were calculated, and their agreement with observations are shown in Fig. 1-A. The residuals, e.g., the difference between experimental and predicted responses, could be utilised to investigate the adequacy of the model [38,39]. Based on a normal distribution, residuals are considered unexplained variations distributed randomly around zero if the model is a good predictor (Fig. 1-S). Thus, the RMS model predicts the observations adequately for the aquifer in the dry climatic zone (Sri Lanka).

The production of coagulants by electrocoagulation depends on electrolysis time and current, which determines the size of the gas bubbles generated at the cathode [40]. Variations of hardness and fluoride removal efficiency as a function of current density and contact time for the water collected from L-1 are shown in Fig. 2-A and B (similar trends of hardness removal were observed for L-2, hence not shown). The contour patterns of hardness and fluoride removals to current density and process time differ markedly. At a given process time, the hardness removal efficiency does not vary significantly with the current density. At a given current density, the hardness removal efficiency monotonously increases with the processing time. However, the spatial variation of fluoride removal efficiency shows a variation with the current density and process time reaching a hillock morphology [39]. The removal of hardness inducing species from water occurs on the cathode surface, and the flocs are generated by Al dissolution. Increased
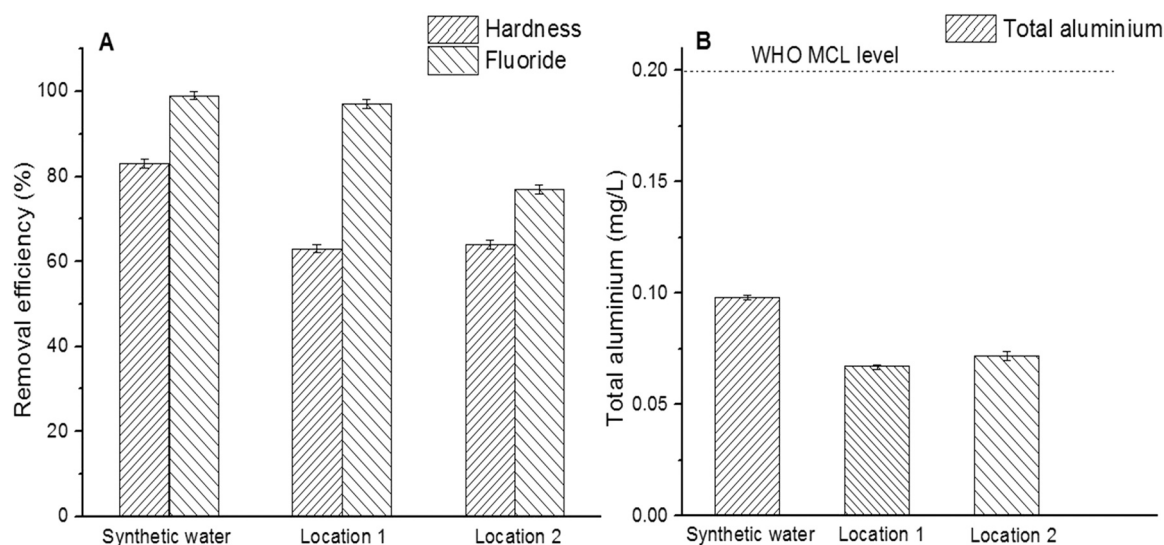
Fig. 3. A. Water hardness and fluoride removal efficiency using optimised EC. B. Residual aluminium concentration in treated water. Feed water composition is shown in Table 1 and Table 1-S. Vertical lines depict error bars.

current density resulted in enhanced OH^- production at the cathode may precipitate Ca^{2+}/Mg^{2+} species on the cathode surface. However, the mass balance calculations show that less than 1% of Ca^{2+} and Mg^{2+} removed on the cathode surface. However, aluminium flocs provide many reactive sites for Ca^{2+} and Mg^{2+} retention [5]. Therefore, hardness removal efficiency is increased above 50 min process time between 4.71 and 5.9 mA/cm^2 current density. Over 80% of fluoride in water can also be removed (Fig. 2-B). However, very high current density values and process time negatively affect hardness (and fluoride) removal efficiencies resulting in a high activity of Al^{3+} free ions [19]. In addition, after the treatment, high density and poor affinity between hydroxide flocs and gas bubbles create a difficultly in floc separation. Because of these reasons, elevated current density and electrolysis time conditions are not suited for hardness removal. Therefore, 3.53 mA/cm^2 current density and 52.2 min time are adequate for optimal removal of hardness (63%) and fluoride (97%) at 1.98 kW h/m^3 energy consumption. The operation cost for removing hardness and fluoride in water by EC is also calculated using the prices of electrode materials (0.76 \$/kg) and electrical energy (0.17 \$/kW h) as input parameters according to the methodology given elsewhere [40]. The hardness and fluoride values of the treated water are 67.3 mg/L $CaCO_3$ and 0.01 mg/L, respectively. Total operation cost is 0.93 US\$/ 0.175 L water.

3.2. Matrix effects on hardness removal

The activities of matrix anions and their chemical nature can change the behaviour of hydrolysed cationic coagulant, directly influencing the hardness removal efficiency. This interaction depends on the changes of electronegativity due to the coordination of aluminium and the replacement of hydroxyl ion or changes of positively charged sites on the metal hydroxide precipitates [41,42]. In the absence of SO_4^{2-}, Cl^-, and NO_3^- in the matrix, the hardness removal efficiency was closed to 80% for simulated water, whereas fluoride removal efficiency was almost above 90% (Fig. 1-B). In each experiment set, a gelatinous deposition layer was observed on the anode surface due to the surface coprecipitation mechanism of defluoridation.

Formation of CaF_2 is possible during the treatment since Ca^{2+} ion concentration is above 150 mg/L [43]. Although $Al_y(OH)_{3x}$ flocs contribute to F^- removal, they also act as a nucleus for the formation of CaF_2. Additionally, a positive effect of Ca^{2+} on fluoride removal was probably associated with the coprecipitation of Al^{3+} and Ca^{2+}.

$$mAl^{3+} + nCa^{2+} + (3m + 2n)H_2O = Al_mCa_n(OH)_{3m+2n} + (3m + 2n)H^+$$
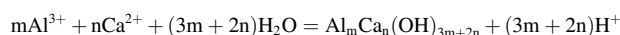
Mg^{2+} also use as a co-coagulant with aluminium salts. However, there is a possibility of forming $Mg(OH)_2$ on the $Al_y(OH)_{3x}$ surface. Therefore, $Mg(OH)_2$ blind the $Al_y(OH)_{3x}$ flocs [44,45]. Stoichiometric coefficients related to the reactions were denoted in m,n,x and y terms.

However, we have noted a negligible mass loss of the cathode at the end of a treatment cycle. The pH values of both source and treated water lie between 6.50 and 7.00. The negligible pH variations of the treated and source waters are ascribed to the high buffer capacity of newly formed polymeric aluminium colloids in neutralising OH^- released at the cathode [19]. Therefore, additional pH adjustment is not required to obtain the highest hardness and fluoride removal efficiency [43]. The situation is markedly different when hardness removal is accounted for via EC treatment with the groundwater (Fig. 1-B). Typically, a natural water system consists of coexisting anions, cations and natural organic matter. Therefore, removing hardness in natural water is complicated compared to simulated water with a controlled matrix. However, simulated water with coexisting ions, viz. NO_3^-, SO_4^{2-}, Cl^- and F^-, hardness removal efficiency values are somewhat similar to the groundwater.

Nitrate does not significantly influence destabilization with aluminium coagulants due to its weak coordination tendency with metal ions. However, chloride and sulphate considerably affect coagulation by aluminium salts [42]. Hardness removal efficiency for simulated water with sulphate anion was comparatively low than other coexisting anions. Therefore, according to Fig. 1-B, our data implied a strong coordination effect of sulphate to the aluminium hydroxide system [27]. Due to the surface ionisation and site-specific complex formation reactions, sulphate anion can destabilise the positively charged aluminium hydrolysis products [41].

Further, the formation of CaF_2 is also reduced, and therefore hardness removal efficiency decreases with increasing the amount of sulphate [33]. Inhibition of aluminium electrode corrosion and competition between sulphate and fluoride ion negatively affect defluoridation efficiency. Therefore, reduced fluoride removal efficiency can be identified with high sulphate containing feed water.

$$Al(OH)_{3-x}F_x + ySO_4^{2-} = Al(OH)_{3-x}F_{x-2y}(SO_4)_y + 2yF^-$$

The negligible effect can be identified with Cl^- ions during defluoridation [43]. Research is needed to assess the role of natural organic matter on floc formation and hardness removal efficiency determinations. The matrix of the solution affects hardness removal
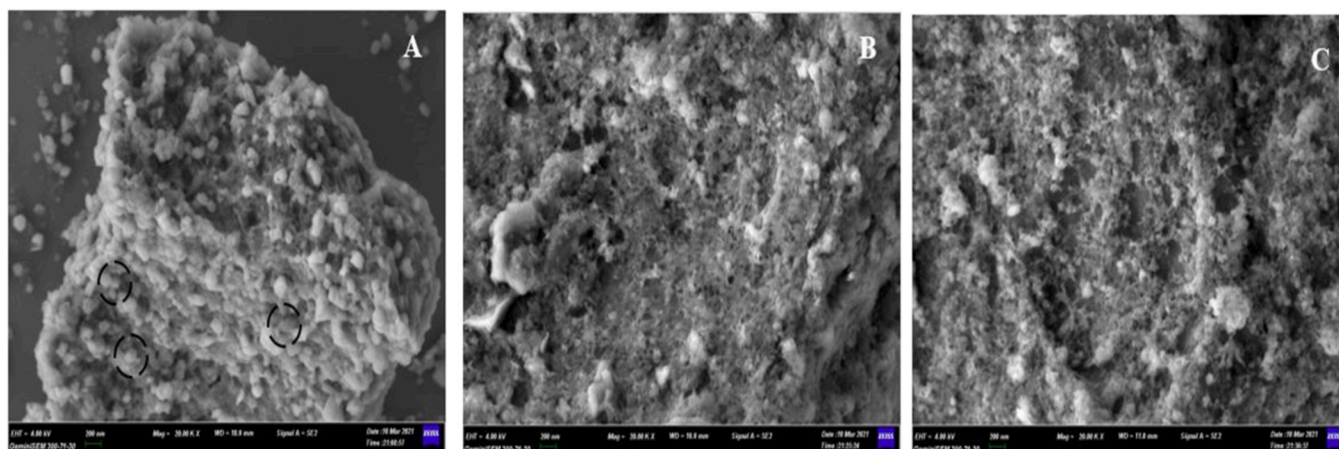
Fig. 4. Scanning electron micrographs obtained for sludge generated after interacting with feed water of different composition. A. F^-/Al feed water, B. Ca^{2+}, Mg^{2+}/Al feedwater C. Ca^{2+}, Mg^{2+}, F^-/Al feedwater.
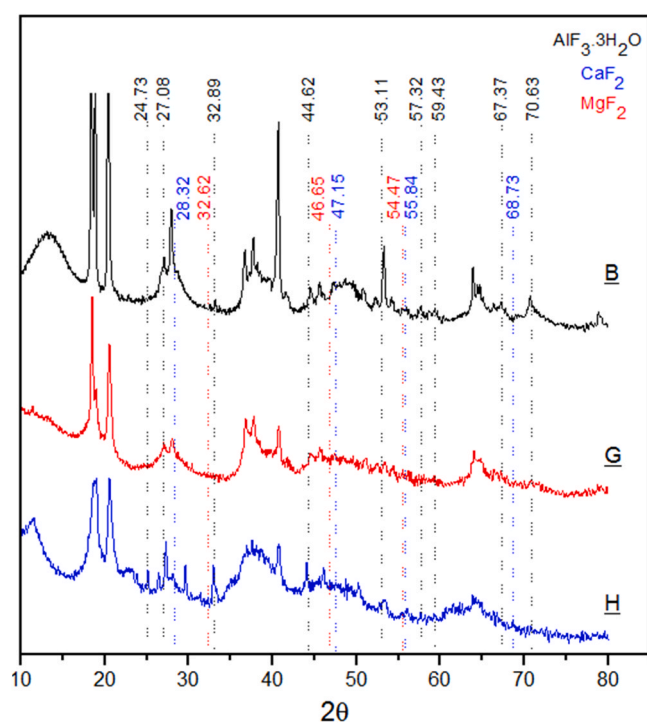

Fig. 5. XRD patterns EC sludge after interacting with feed water of different composition. B: fluoride feedwater G: hardness feedwater and H: hardness and fluoride feedwater.

efficiency. Therefore simulated water removal efficiency is not matched with the developed model as contaminated water. The removal efficiencies of fluoride and hardness in different water types using optimised EC reactor are shown in Fig. 3.A. The residual aluminium concentration in treated water is always below the WHO maximum contaminant levels (MCL) as shown in Fig. 3. B [46].

3.3. Sludge characterisation

3.3.1. SEM characterisation

SEM images were used to investigate the morphology of optimised condition sludge (Fig. 4). The Al sludge generated by fluoride treatment shows spherical and porous nanoparticles consist of aluminium oxide hydroxide species (black circles in Fig. 4. A) [47]. However, in the optimised sludge of Ca^{2+}, Mg^{2+} /Al and Ca^{2+}, Mg^{2+}, F^-/Al superb

porosity can be identified with a large surface area. Additionally, amorphous sludge particulates are also present.

3.3.2. XRD characterisation

By the dissolution of Al sacrificing anode in EC, the Al-sludge is generated. The chemical composition and the structure of the sludge depend on the feed solution composition. The XRD data of Al derived sludge generated in the EC cell upon interactions with hard water in the presence or absence of F^- are shown in Fig. 5. The XRD peaks at $2\theta^0$ 18.59^0, 20.44^0, 26.33^0, 50.65^0, and 52.36^0 confirmed gelatinous $Al_y(OH)_{3x}$ sludge phase believed to form via Al_{13} kegging in monopolar EC configuration [48,49]. When $Al_y(OH)_{3x}$ derived sludge interacts with hard water, carbonate and hydroxide phases of calcium and magnesium also emerge. The peaks at $2\theta = 23.88^0$, 29.36^0, 36.5^0, 39.5^0, 48.5^0, 56.6^0 correspond to the calcium carbonate phase readily discern in the Al-sludge generated by fluoride hard water treatment [50]. $AlF_3.3 H_2O$, CaF_2, and MgF_2 phases can also be identified when Al-derived sludge interacts with hard water enriched with fluoride. Sharp diffraction peaks correspond to $AlF_3.3 H_2O$ are identified at $2\theta = 24.73^0$, 27.08^0, 32.89^0, 44.62^0, 53.11^0, 57.32^0, 59.43^0, 67.36^0, 70.63^0 [51]. The peaks at 2θ $= 15.15^0$, 30.39^0, 48.70^0 confirm the presence of aluminium fluoride hydroxide [29]. The relative intensity of XRD peaks correspond to $Al_y(OH)_{3x}$ has reduced when Ca^{2+} and Mg^{2+} is present in association with F^-. The reduced XRD peak intensity of the sludge confirms the improved defluoridation in the presence of Ca^{2+} and Mg^{2+}. Therefore, the cubic phase of the fluorite (CaF_2 space group Fm3m) can be identified. The XRD peaks at $2\theta = 28.32^0$, 47.15^0, 55.84^0, 68.73^0 corresponded to (111), (202), (311) and (400) planes, respectively [29,52]. The diffraction peaks at $2\theta = 32.62^0$, 46.65^0, 54.47^0 confirm the MgF_2 phase in the sludge [53].

3.3.3. XPS characterisation

The high-resolution x-ray photoelectron spectroscopic spectrums of O_{1s}, C_{1s}, Al_{2p}, Ca_{2p}, Mg_{1s}, and F_{1s} received by interacting EC sludge with feed solution containing Ca^{2+}, Mg^{2+} and F^- is shown in Fig. 6. The Al_{2p} peak at 74.27 eV is ascribed to $Al_y(OH)_{3x}$ phase [54]. The O_{1s} peak at 531.8 eV occurs due to bulk hydroxyls in $Al_y(OH)_{3x}$ phase [54]. The observed $\left(\frac{O}{Al}\right)$ atomic ratio ~ 3 favours $Al_y(OH)_{3x}$ stoichiometry (Table 4-S). As EC process time evolved, the aggregation of gelatinous $Al_y(OH)_{3x}$ particulates is discerned, and the formation of γ-AlO(OH) phase with high crystallinity is favoured, as supported by the reduced $\left(\frac{O}{Al}\right)$ ratio. The peak at 75.48 eV due to Al in fluorinated alumina ($AlOF_x$) supports fluoride removal on aluminium oxide hydroxide
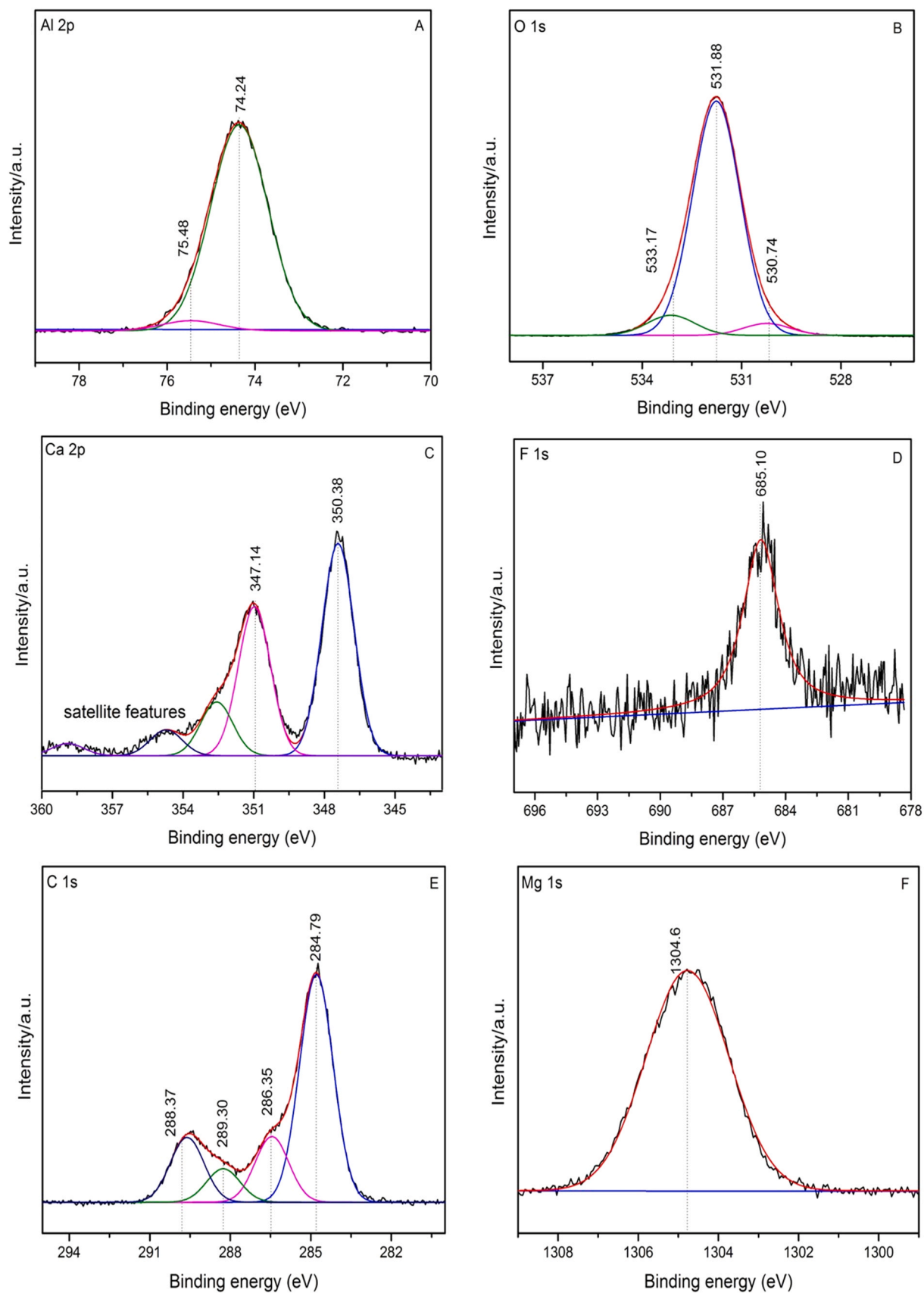
Fig. 6. XPS curve fit of Al2p, O1s, C1s, Ca2p, F1s and Mg1s spectrum of optimised condition Ca^{2+}, Mg^{2+}, F^-/Al sludge. The elemental composition data of the sludge materials is given in Table 4-S.
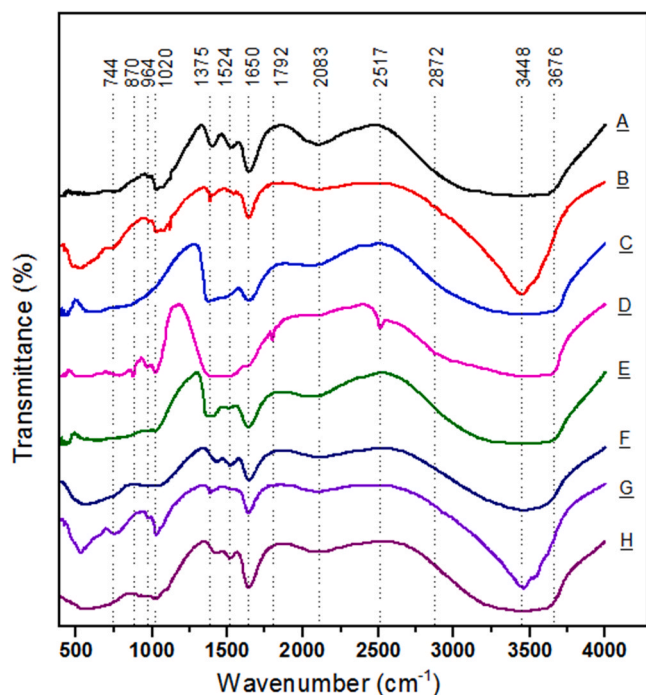
Fig. 7. FTIR spectra of A: aluminium sludge B: sludge with F⁻ C: sludge with Mg²⁺ D: sludge with Ca²⁺ E: sludge with Mg²⁺ and F⁻ F: sludge with ca²⁺ and F⁻ G: sludge with Ca²⁺ and Mg²⁺ H: simultaneous hardness (Ca²⁺, Mg²⁺) and fluoride sludge.
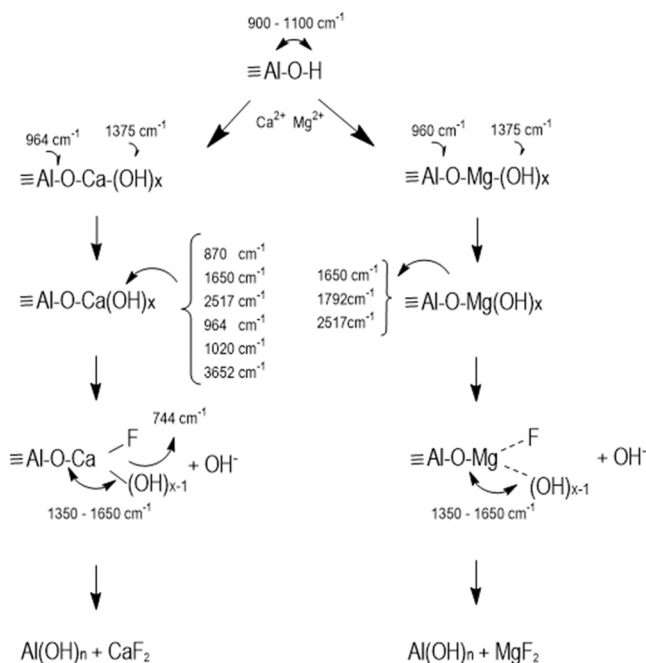

Fig. 8. A postulated mechanism for concurrent removal of fluoride and hardness in water by EC. Double-headed arrows represent possible bending vibrations in proposed species.

substrate [55] (Fig. 6. A). The XPS spectrum of O_{1s} has resolved into three peaks. The peak at 530.74 eV binding energy is ascribed to lattice oxygen in Al_2O_3 [56]. The adsorbed water on sludge creates a peak at 533.17 eV [54,56] (Fig. 6. B). The spin-orbit doublet of Ca 2p is observed at binding energies of 347.14 eV for $Ca_{2p\ 3/2}$ and 350.68 eV for $Ca_{2p\ 1/2}$. These peaks are assigned to CaF_2, associated with ≡Ca-O and ≡Ca-OH sites [57,58]. The difference in binding energy between $Ca_{2p\ 3/2}$ and $Ca_{2p\ 1/2}$ bands is 0.8 eV [59]. This value increases as a function of O^{2-} and OH^- species (Fig. 6. C). The F_{1s} peak at 685.10 eV indicates CaF_2 in the contaminated sludge [58]. The peculiar behaviour of the peak in the vicinity of ~685 eV confirms fluoride removal as CaF_2, but not as AlF_3 [59] (Fig. 6. D).

The C 1s peak at 289.30 eV confirmed the presence of carbonate in the sludge [60] (Fig. 6. E). In agreement with XRD spectra, the Ca 2p peak has spaced spin-orbit components related to ΔC carbonate = 3.54 and interaction of CaF_2 species with $CaCO_3$ in the Ca²⁺, Mg²⁺, F⁻/Al sludge [61]. Additionally, the strong satellite features further confirm the presence of $CaCO_3$ species in the Ca²⁺, Mg²⁺, F⁻/Al sludge [62]. In Mg 1s spectrum, the peak at a binding energy of 1304.6 eV implied the metal carbonate [63] (Fig. 6. F). Further, O 1s spectrum of Ca²⁺, Mg²⁺, F⁻/Al sludge indicates carbonate at a binding energy of 533.17 eV with C 1s spectra at a binding energy of 289.30 eV [64]. The $\frac{[O]}{[Mg]}$ atomic percentage for Ca²⁺, Mg²⁺ /Al sludge was 12.10 while 16.28 for Ca²⁺, Mg²⁺,F⁻/Al sludge (Table 4-S). The sludge with high oxygen content implied the presence of oxygen contain debris. Therefore, there is Mg²⁺ in MgO, $Mg(OH)_2.nH_2O$ and $MgCO_3$ forms [65].

3.3.4. FTIR characterisation

The discrete IR bands are shown in the lattice vibration region, i.e., 1200–1800 cm⁻¹ are ascribed to admixture CO_2 or H_2O adsorption on Al-derived sludge (Fig. 7. A). The variations in these IR bands provide important information between surface sites and solute species interactions. The IR bands shown in the 900–1100 cm⁻¹ range is due to the formation of gelatinous $\equiv Al_y(OH)_{3x}$ colloids (Fig. 7. A). The formation of gelatinous $\equiv Al_y(OH)_{3x}$ was observed in experiments. The IR

band at 1650 cm⁻¹ due to H-O-H bending vibrations confirms the presence of surface-adhered water on $\equiv Al_y(OH)_{3x}$ [66]. The bands at 3676 cm⁻¹ and 3448 cm⁻¹ persist even after the evacuation, can be ascribed to -OH stretching and H-bonded -OH vibrations of ≡ AlOH [67]. Further, the appearance of a band at 1524 cm⁻¹ suggests the presence of surface ≡ AlOH bending vibrations. The IR spectrum in Fig. 7. B was measured after interactions of F⁻ with $\equiv Al_y(OH)_{3x}$. A new IR band appeared at 744 cm⁻¹, and the band at 1020 cm⁻¹ due to $\equiv Al-O-H$ deformation vibration shifted to higher wavenumber [68, 69], and band at 1375 cm⁻¹ decreased in intensity while the band at 1524 cm⁻¹ ascribed to the $\equiv Al-O-H$ bending vibrations disappeared due to $OH^- \rightarrow F^-$ substitution [29,69]. The emergence of a band at 744 cm⁻¹ can be ascribed to the $Al-F$ vibrations in ≡ AlF(OH) complexes [69–71]. When Mg²⁺ ions were added to the initial sludge, as shown in Fig. 7. C, the IR bands around 1000 cm⁻¹ and 1380 cm⁻¹ broaden due to weak interactions between Al-sludge and magnesium species forming few $\equiv Al-O-Mg-OH$. As evidenced from Fig. 7. D, compared to Mg²⁺, the interactions with Ca²⁺ and Al-sludge show distinct features at 870 cm⁻¹ and 964 cm⁻¹ that can be ascribed to $Al-O-Ca-OH$ formation ($\equiv Al-O-Ca-OH)^{\delta+}$ species. Further, the appearance of distinct bands at 1792 cm⁻¹ and 2517 cm⁻¹ may be due to the resonance of the band at 870 cm⁻¹. When F⁻ ions were introduced to the sludge-Mg system, the re-appearance of very small bands around 1020 cm⁻¹ and 1380 cm⁻¹ indicates the release of some H-bonding behaviour of $\equiv Al-O-Mg-OH$ species, probably due to the formation of $\equiv MgF-OH$ species as evident in Fig. 7. E [72].

These changes are prominent in the spectrum Fig. 7. E, which is obtained with the interaction of F⁻ ions with the sludge-Ca system, indicating CaF−OH species' formation together with ≡ CaF. The formation of direct ≡ CaF species can be confirmed by observing the disappearance of bands in the 900–1100 cm⁻¹ range of the spectrum Fig. 7.D. This has been further supported by the observation of the reduction of H-bonding nature in the spectrum Fig. 7. F where some small distinct features appeared around 3600 cm⁻¹ freeing OH species indicating the replacement of more OH groups by F⁻. When Ca²⁺, Mg²⁺ interact simultaneously with the sludge (Fig. 7. G), the spectral features related to Ca²⁺ interactions are predominant over the Mg²⁺ interactions;

when F^- is added to the above system formation of more $\equiv CaF - OH$ and $\equiv CaF$ sites compared to $\equiv MgF - OH$ species is evident as the spectra of Fig. 7. F and Fig. 7. H are quite similar to each other. The XRD and XPS analyses confirm CaF_2, MgF_2 and $AlF_3.3H_2O$ phases in the EC sludge resulted by different feed waters. Commitment fluoride and hardness removal mechanism by EC is shown in Fig. 8.

4. Conclusions

The chemical nature of the solution matrix exerts significantly on hardness and fluoride removal efficiency by electrocoagulation. A maximum of 83% hardness and 99% fluoride removal efficiencies were achieved for simulated water within 28 min, consuming a total of 0.69 kW h m^{-3} energy. The presence of residual Al^{3+} in treated water limits its direct consumption. Further research is necessary to identify aluminium species in water after simultaneous hardness and fluoride removal by electrocoagulation.

CRediT authorship contribution statement

J.U. Halpegama: Methodology, Writing – original draft, **K.Y. Heenkenda**: Investigation, Validation, **Zhiguo Wu**: Visualization, **K.G. N. Naanaykkara**: Resources, **R.M.G. Rajapakse**: Supervision, **A. Bandara**: Data curation, **Ajith C. Herath**: Supervision, Validation, **Xing Chen**: Conceptualization, Formal analysis, Funding acquisition, Project administration, Resources, Writing – review & editing, **Rohan Weerasooriya**: Conceptualization, Funding acquisition, Project administration, Writing – review & editing.

Declaration of Competing Interest

The authors declare that they have no known competing financial interests or personal relationships that could have appeared to influence the work reported in this paper.

Acknowledgements

Appendix A. Supporting information

Supplementary data associated with this article can be found in the online version at doi:10.1016/j.jece.2021.106105.

References

[1] D. Dimkić, Temperature impact on drinking water consumption, Environ. Sci. Proc. 2 (2020) 31, https://doi.org/10.3390/environsciproc2020002031.

[2] S.D. Mengesha, A. Weldetinsae, K. Tesfaye, G. Taye, Organoleptic and palatability properties of drinking water sources and its health implications in Ethiopia: a retrospective study during 2010-2016, Environ. Heal. Eng. Manag. 5 (2018) 221–229, https://doi.org/10.15171/ehem.2018.30.

[3] I.A. Abboud, Geochemistry and quality of groundwater of the Yarmouk basin aquifer, North Jordan, Environ. Geochem. Health 40 (2017) 1405–1435, https://doi.org/10.1007/s10653-017-0064-x.

[4] C. Montero-Ocampo, J.F.M. Villafañe, Effect of dissolved species on the fluoride electro-removal from groundwater, ECS Trans. 28 (2010) 57–65.

[5] S.L. Zhi, K.Q. Zhang, Hardness removal by a novel electrochemical method, Desalination 381 (2016) 8–14, https://doi.org/10.1016/j.desal.2015.12.002.

[6] J.S. Park, J.H. Song, K.H. Yeon, S.H. Moon, Removal of hardness ions from tap water using electromembrane processes, Desalination 202 (2007) 1–8, https://doi.org/10.1016/j.desal.2005.12.031.

[7] D.L. Sedlak, The unintended consequences of the reverse osmosis revolution, Environ. Sci. Technol. 53 (2019) 3999–4000, https://doi.org/10.1021/acs.est.9b01755.

[8] A.M. Naser, M. Shamsudduha, T.F. Clasen, K.M.V. Narayan, Letter to the editor regarding 'the unintended consequences of the reverse osmosis revolution',

Environ. Sci. Technol 53 (2019) 7173–7174, https://doi.org/10.1021/acs.est.9b02917.

[9] L. Birnhack, O. Keller, S.C.N. Tang, N. Fridman-Bishop, O. Lahav, A membrane-based recycling process for minimizing environmental effects inflicted by ion-exchange softening applications, Sep. Purif. Technol. 223 (2019) 24–30, https://doi.org/10.1016/j.seppur.2019.04.056.

[10] J. Wen, H. Dong, G. Zeng, Application of zeolite in removing salinity/sodicity from wastewater: a review of mechanisms, challenges and opportunities, J. Clean. Prod. 197 (2018) 1435–1446, https://doi.org/10.1016/j.jclepro.2018.06.270.

[11] M. Sillanpää, M. Shestakova, Electrochemical water treatment methods, 2017. https://doi.org/10.1016/B978-0-12-811462-9.00002-5.

[12] M.A.C.K. Hansima, M. Makehelwala, K.B.S.N. Jinadasa, Y. Wei, K.G. N. Nanayakkara, A.C. Herath, R. Weerasooriya, Fouling of ion exchange membranes used in the electrodialysis reversal advanced water treatment: a review, Chemosphere 263 (2021), 127951, https://doi.org/10.1016/j.chemosphere.2020.127951.

[13] S.V. Jadhav, E. Bringas, G.D. Yadav, V.K. Rathod, I. Ortiz, K.V. Marathe, Arsenic and fluoride contaminated groundwaters: a review of current technologies for contaminants removal, J. Environ. Manag. 162 (2015) 306–325, https://doi.org/10.1016/j.jenvman.2015.07.020.

[14] D. Clímaco Patrocínio, C.C. Neves Kunrath, M.A. Siqueira Rodrigues, T. Benvenuti, F. Dani Rico Amado, Concentration effect and operational parameters on electrodialysis reversal efficiency applied for fluoride removal in groundwater, J. Environ. Chem. Eng. 7 (2019), 103491, https://doi.org/10.1016/j.jece.2019.103491.

[15] N.B. Goodman, R.J. Taylor, Z. Xie, Y. Gozukara, A. Clements, A feasibility study of municipal wastewater desalination using electrodialysis reversal to provide recycled water for horticultural irrigation, Desalination 317 (2013) 77–83, https://doi.org/10.1016/j.desal.2013.02.010.

[16] L.J. Banasiak, A.I. Schäfer, Removal of boron, fluoride and nitrate by electrodialysis in the presence of organic matter, J. Memb. Sci. 334 (2009) 101–109, https://doi.org/10.1016/j.memsci.2009.02.020.

[17] T. Kim, T.K. Kim, K.D. Zoh, Removal mechanism of heavy metal (Cu, Ni, Zn, and Cr) in the presence of cyanide during electrocoagulation using Fe and Al electrodes, J. Water Process Eng. 33 (2020), 101109, https://doi.org/10.1016/j.jwpe.2019.101109.

[18] D. Mills, New process for electrocoagulation, J./Am. Water Work. Assoc. 92 (2000) 34–43, https://doi.org/10.1002/j.1551-8833.2000.tb08957.x.

[19] J.N. Hakizimana, B. Gourich, M. Chafi, Y. Stiriba, C. Vial, P. Drogui, J. Naja, Electrocoagulation process in water treatment: a review of electrocoagulation modeling approaches, Desalination 404 (2017) 1–21, https://doi.org/10.1016/j.desal.2016.10.011.

[20] K. Padmaja, J. Cherukuri, M. Anji Reddy, A comparative study of the efficiency of chemical coagulation and electrocoagulation methods in the treatment of pharmaceutical effluent, J. Water Process Eng. 34 (2020), 101153, https://doi.org/10.1016/j.jwpe.2020.101153.

[21] N. Boudjema, N. Drouiche, N. Abdi, H. Grib, H. Lounici, A. Pauss, N. Mameri, Treatment of Oued El Harrach river water by electrocoagulation noting the effect of the electric field on microorganisms, J. Taiwan Inst. Chem. Eng. 45 (2014) 1564–1570, https://doi.org/10.1016/j.jtice.2013.10.006.

[22] R. Niazmand, M. Jahani, F. Sabbagh, S. Rezania, Optimization of electrocoagulation conditions for the purification of table olive debittering wastewater using response surface methodology, Water 12 (2020) 1687, https://doi.org/10.3390/W12061687.

[23] C.A. Martínez-Huitle, Environment-friendly electrochemical processes, Materials (2021) 1548, https://doi.org/10.3390/ma14061548.

[24] B. Palahouane, N. Drouiche, S. Aoudj, K. Bensadok, Cost-effective electrocoagulation process for the remediation of fluoride from pretreated photovoltaic wastewater, J. Ind. Eng. Chem. 22 (2015) 127–131, https://doi.org/10.1016/j.jiec.2014.06.033.

[25] I. Kabdaşlı, I. Arslan-Alaton, T. Ölmez-Hancı, O. Tünay, Electrocoagulation applications for industrial wastewaters: a critical review, Environ. Technol. Rev. 1 (2012) 2–45, https://doi.org/10.1080/21622515.2012.715390.

[26] J. Parthasarathy, N, Buffle, Study of polymeric aluminium (III) hydroxide solutions for application in waste water treatment. Properties of the polymer and optimal conditions of preparation, Water Res. 19 (1985) 25–36.

[27] J. Duan, J. Gregory, Coagulation by hydrolysing metal salts, Adv. Colloid Interface Sci. 100–102 (2003) 475–502, https://doi.org/10.1016/S0001-8686(02)00067-2.

[28] P. Song, Z. Yang, H. Xu, J. Huang, X. Yang, L. Wang, Investigation of influencing factors and mechanism of antimony and arsenic removal by electrocoagulation using Fe-Al electrodes, Ind. Eng. Chem. Res. 53 (2014) 12911–12919, https://doi.org/10.1021/ie501727a.

[29] S. Aoudj, A. Khelifa, N. Drouiche, R. Belkada, D. Miroud, Simultaneous removal of chromium(VI) and fluoride by electrocoagulation-electroflotation: application of a hybrid Fe-Al anode, Chem. Eng. J. 267 (2015) 153–162, https://doi.org/10.1016/j.cej.2014.12.081.

[30] A. Guzmán, J.L. Nava, O. Coreño, I. Rodríguez, S. Gutiérrez, Arsenic and fluoride removal from groundwater by electrocoagulation using a continuous filter-press reactor, Chemosphere 144 (2016) 2113–2120, https://doi.org/10.1016/j.chemosphere.2015.10.108.

[31] A.R. Amani-Ghadim, S. Aber, A. Olad, H. Ashassi-Sorkhabi, Optimization of electrocoagulation process for removal of an azo dye using response surface methodology and investigation on the occurrence of destructive side reactions, Chem. Eng. Process. Process. Intensif. 64 (2013) 68–78, https://doi.org/10.1016/j.cep.2012.10.012.

[32] M. Ahmadi, F. Vahabzadeh, B. Bonakdarpour, E. Mofarrah, M. Mehranian, Application of the central composite design and response surface methodology to the advanced treatment of olive oil processing wastewater using Fenton's peroxidation, J. Hazard. Mater. 123 (2005) 187–195, https://doi.org/10.1016/j.jhazmat.2005.03.042.

[33] U. Tezcan Un, A.S. Koparal, U. Bakir Ogutveren, Fluoride removal from water and wastewater with a bach cylindrical electrode using electrocoagulation, Chem. Eng. J. 223 (2013) 110–115, https://doi.org/10.1016/j.cej.2013.02.126.

[34] P. Sarojam, Analysis of wastewater for metals using ICP-OES, 2010. ⟨http://www.perkinelmer.com/lab-solutions/resources/docs/APP_MetalsinWastewater.pdf⟩ (viewed on 17-07-2021).

[35] F.S. Stover, R.V. Brill, Statistical quality control applied to ion chromatography calibrations, J. Chromatogr. A 804 (1998) 37–43, https://doi.org/10.1016/S0021-9673(98)00094-6.

[36] P. Jackson, Ion chromatography in environmental analysis., 2006. https://doi.org/10.1002/9780470027318.a0835.

[37] A. Asfaram, M. Ghaedi, S. Agarwal, I. Tyagi, V.K. Gupta, Removal of basic dye Auramine-O by ZnS:Cu nanoparticles loaded on activated carbon: optimization of parameters using response surface methodology with central composite design, RSC Adv. 5 (2015) 18438–18450, https://doi.org/10.1039/c4ra15637d.

[38] I.H. Cho, K.D. Zoh, Photocatalytic degradation of azo dye (Reactive Red 120) in TiO2/UV system: optimization and modeling using a response surface methodology (RSM) based on the central composite design, Dye Pigment 75 (2007) 533–543, https://doi.org/10.1016/j.dyepig.2006.06.041.

[39] M. Behbahani, M.R.A. Moghaddam, M. Arami, Techno-economical evaluation of fluoride removal by electrocoagulation process: optimization through response surface methodology, Desalination 271 (2011) 209–218, https://doi.org/10.1016/j.desal.2010.12.033.

[40] M. Kobya, E. Demirbas, F. Ulu, Evaluation of operating parameters with respect to charge loading on the removal efficiency of arsenic from potable water by electrocoagulation, J. Environ. Chem. Eng. 4 (2016) 1484–1494, https://doi.org/10.1016/j.jece.2016.02.016.

[41] R.D. Letterman, S.G. Vanderbrook, Effect of solution chemistry on coagulation with hydrolyzed Al(III). Significance of sulfate ion and pH, Water Res. 17 (1983) 195–204, https://doi.org/10.1016/0043-1354(83)90100-8.

[42] G.P. Hanna Jr., A.J. Rubin, Effect of sulfate and other ions in coagulation with aluminum (III), J.-Am. Water Work. Assoc. 62 (1970) 315–321, https://doi.org/10.1002/j.1551-8833.1970.tb03912.x.

[43] Q. Zuo, X. Chen, W. Li, G. Chen, Combined electrocoagulation and electroflotation for removal of fluoride from drinking water, J. Hazard. Mater. 159 (2008) 452–457, https://doi.org/10.1016/j.jhazmat.2008.02.039.

[44] F. Shen, X. Chen, P. Gao, G. Chen, Electrochemical removal of fluoride ions from industrial wastewater, Chem. Eng. Sci. 58 (2003) 987–993, https://doi.org/10.1016/S0009-2509(02)00639-5.

[45] H. Zhao, B. Zhao, W. Yang, T. Li, Effects of Ca2+ and Mg2+ on defluoridation in the electrocoagulation process, Environ. Sci. Technol. 44 (2010) 9112–9116, https://doi.org/10.1021/es102540t.

[46] World Health Organization (WHO), Aluminium in drinking-water: background document for development of WHO Guidelines for drinking-water quality, 1998. ⟨http://www.who.int/es/⟩ (viewed on 17-07-2021).

[47] S. Tanada, M. Kabayama, N. Kawasaki, T. Sakiyama, T. Nakamura, M. Araki, T. Tamura, Removal of phosphate by aluminum oxide hydroxide, J. Colloid Interface Sci. 257 (2003) 135–140, https://doi.org/10.1016/S0021-9797(02)00008-5.

[48] M. Saalfeld, H, Wedde, Refinement of the crystal structure of gibbsite, A1(OH)3, Zeitschrift Für Krist, Mater 139 (1974) 129–135.

[49] H.D. Megaw, The crystal structure of hydrargillite, Al(OH)3, Z. Kristallogr. Mater. 87 (1934) 185–205.

[50] V. Apalangya, V. Rangari, B. Tiimob, S. Jeelani, T. Samuel, Development of antimicrobial water filtration hybrid material from bio source calcium carbonate and silver nanoparticles, Appl. Surf. Sci. 295 (2014) 108–114, https://doi.org/10.1016/j.apsusc.2014.01.012.

[51] E.H.E. Marlene C. Morris, Howard F. McMurdie, D.M.G. Boris Paretzkin, Harry S. Parker, Winnie Wong-Ng, Standard X-ray diffraction powder patterns section 21 — data for 92 substances, National Bureau of Standards Monograph 25 Washington p. 148, 1985.

[52] M. Schreyer, M. Guo, L. Thirunahari, S. Gao, F, Garland, Simultaneous determination of several crystal structures from powder mixtures: the combination of powder X-ray diffraction, band-target entropy minimization and Rietveld methods, J. Appl. Crystallogr. 47 (2014) 659–667.

[53] Z.Q. Haines, J. Leger, J.M. Gorelli, F. Klug, D.D. Tse, J.S, Li, X-ray diffraction and theoretical studies of the high-pressure structures and phase transitions in magnesium fluoride, Phys. Rev. B 64 (2001) 1341101–13411010, https://doi.org/10.1103/PhysRevB.64.134110.

[54] S. Chellam, P. Gamage, T. Tanneru, M.A. Sari, Aluminum electrocoagulation and electroflotation pretreatment for microfiltration: fouling reduction and improvements in filtered water quality, in: Desalin. Water Purif. Res. Dev. Progr., 2014: pp. 1–114. ⟨https://www.usbr.gov/research/dwpr/DWPR_Reports.html⟩ (viewed on 17-07-2021).

[55] R. Ramos, G. Cunge, B. Pelissier, O. Joubert, Cleaning aluminum fluoride coatings from plasma reactor walls in SiCl4/Cl2 plasmas, Plasma Sources Sci. Technol. 16 (2007) 711–715, https://doi.org/10.1088/0963-0252/16/4/004.

[56] D. Sun, X. Hong, K. Wu, K.S. Hui, Y. Du, K.N. Hui, Simultaneous removal of ammonia and phosphate by electro-oxidation and electrocoagulation using RuO2–IrO2/Ti and microscale zero-valent iron composite electrode, Water Res. 169 (2020), 115239, https://doi.org/10.1016/j.watres.2019.115239.

[57] R. Bennewitz, M. Reichling, R.M. Wilson, R.T. Williams, K. Holldack, M. Grunze, E. Matthias, Characterization of Ca aggregates on CaF2 (111)-surfaces by atomic force, XPS, and fluorescence microscopy, Nucl. Inst. Methods Phys. Res. B 91 (1994) 623–627, https://doi.org/10.1016/0168-583X(94)96298-7.

[58] A.B. Christie, J. Lee, I. Sutherland, J.M. Walls, An XPS study of ion-induced compositional changes with group II and group IV compounds, Appl. Surf. Sci. 15 (1983) 224–237, https://doi.org/10.1016/0378-5963(83)90018-1.

[59] C. dos, S. Bezerra, M.E.G. Valerio, Structural and optical study of CaF2 nanoparticles produced by a microwave-assisted hydrothermal method, Phys. B Condens. Matter 501 (2016) 106–112, https://doi.org/10.1016/j.physb.2016.08.025.

[60] D.R. Baer, J.F. Moulder, High resolution XPS spectrum of calcite (CaCO3), Surf. Sci. Spectra 2 (1993) 1–7, https://doi.org/10.1116/1.1247719.

[61] T. Roychowdhury, S. Bahr, P. Dietrich, M. Meyer, A. Thißen, M.R. Linford, Calcite (CaCO3), by near-ambient pressure XPS, Surf. Sci. Spectra 26 (2019), 014025, https://doi.org/10.1116/1.5109266.

[62] C.S. Gopinath, S.G. Hegde, A.V. Ramaswamy, S. Mahapatra, Photoemission studies of polymorphic CaCO3 materials, Mater. Res. Bull. 37 (2002) 1323–1332, https://doi.org/10.1016/S0025-5408(02)00763-8.

[63] F. Khairallah, A. Glisenti, XPS study of MgO nanopowders obtained by different preparation procedures, Surf. Sci. Spectra 13 (2006) 58–71, https://doi.org/10.1116/11.20060601.

[64] M. Santamaria, F. Di Quarto, S. Zanna, P. Marcus, Initial surface film on magnesium metal: a characterization by X-ray photoelectron spectroscopy (XPS) and photocurrent spectroscopy (PCS), Electrochim. Acta 53 (2007) 1314–1324, https://doi.org/10.1016/j.electacta.2007.03.019.

[65] A. Hamwi, C. Latouche, V. Marchand, J. Dupuis, R. Benoit, Perfluorofullerenes: characterization and structural aspects, J. Phys. Chem. Solids 57 (1996) 991–998.

[66] E. Balan, M. Lazzeri, G. Morin, F. Mauri, First-principles study of the OH-stretching modes of gibbsite, Am. Mineral. 91 (2006) 115–119, https://doi.org/10.2138/am.2006.1922.

[67] L. Chen, H.X. Wu, T.J. Wang, Y. Jin, Y. Zhang, X.M. Dou, Granulation of Fe-Al-Ce nano-adsorbent for fluoride removal from drinking water by spray coating on sand in a fluidized bed, Powder Technol. 193 (2009) 59–64, https://doi.org/10.1016/j.powtec.2009.02.007.

[68] C. Morterra, G. Magnacca, A case study: surface chemistry and surface structure of catalytic aluminas, as studied by vibrational spectroscopy of adsorbed species, Catal. Today 27 (1996) 497–532, https://doi.org/10.1016/0920-5861(95)00163-8.

[69] R. Liu, W. Gong, H. Lan, Y. Gao, H. Liu, J. Qu, Defluoridation by freshly prepared aluminum hydroxides, Chem. Eng. J. 175 (2011) 144–149, https://doi.org/10.1016/j.cej.2011.09.083.

[70] R. Liu, W. Gong, H. Lan, T. Yang, H. Liu, J. Qu, Simultaneous removal of arsenate and fluoride by iron and aluminum binary oxide: competitive adsorption effects, Sep. Purif. Technol. 92 (2012) 100–105, https://doi.org/10.1016/j.seppur.2012.03.020.

[71] U. Gross, S. Rüdiger, E. Kemnitz, K.W. Brzezinka, S. Mukhopadhyay, C. Bailey, A. Wander, N. Harrison, Vibrational analysis study of aluminum trifluoride phases, J. Phys. Chem. A 111 (2007) 5813–5819, https://doi.org/10.1021/jp072388r.

[72] S. Wuttke, A. Vimont, J.C. Lavalley, M. Daturi, E. Kemnitz, Infrared investigation of the acid and basic properties of a sol-gel prepared MgF2, J. Phys. Chem. C 114 (2010) 5113–5120, https://doi.org/10.1021/jp911584h.